Journal of Alloys and Compounds 506 (2010) 569–574

Contents lists available at ScienceDirect

Journal of Alloys and Compounds

journal homepage: www.elsevier.com/locate/jallcom

Structural study and properties of a new iron phosphate $Rb_9Fe_7(PO_4)_{10}$

Mourad Hidouri [a,*], Alain Wattiaux [b], María Luisa López [c], Carlos Pico [c], Mongi B. Amara [a]

[a] UR Matériaux Inorganiques, Faculté des Sciences, 5019 Monastir, Tunisia
[b] CNRS, Université de Bordeaux, ICMCB, 87 avenue du Dr. A. Schweitzer, Pessac F-33608, France
[c] Departamento de Química Inorgánica I, Facultad de Ciencias Químicas, Universidad Complutense, 28040 Madrid, Spain

ARTICLE INFO

Article history:
Received 10 May 2010
Received in revised form 23 June 2010
Accepted 10 July 2010
Available online 23 July 2010

Keywords:
Iron phosphate
Chemical synthesis
X-ray diffraction
Magnetic susceptibility
Mössbauer spectroscopy

ABSTRACT

Synthesis, single crystal X-ray diffraction, Mössbauer and magnetic studies of a new iron phosphate $Rb_9Fe_7(PO_4)_{10}$ are described. This compound crystallizes in the monoclinic system with the space group $P2_1/a$ and the following parameters: $a = 9.886(4)$ Å, $b = 16.493(2)$ Å, $c = 13.437(2)$ Å, $\beta = 110.49(3)^\circ$ and $Z = 2$. Its structure is closely related to that of the $Cs_{9-x}K_xFe_7(PO_4)_{10}$ phosphates. The 3D framework consists of FeO_6 and FeO_5 polyhedra and Fe_2O_{10} units of corner-sharing FeO_6 and FeO_5 polyhedra. These units are linked to each other by the phosphate tetrahedra in such a way that the resulting framework forms large intersecting tunnels extending along the *a* and *c* directions, where the Rb^+ cations are located. A high temperature X-ray powder diffraction study showed a partial decomposition of the product above 773 K. The magnetic susceptibility results are consistent with Fe(III) showing an antiferromagnetic ordering below $T_N \approx 19$ K and a paramagnetic behavior in the range of 50–300 K. The application of the Curie–Weiss law yields an effective moment of 5.99 μ_B in a good agreement with the ideal spin only value of 5.92 μ_B for d^5-iron(III). The distribution of iron and its local environments were confirmed by a Mössbauer study undertaken at 293 and 4.2 K.

1. Introduction

Iron monophosphates have interesting applications in several fields. For example, they were successfully used as catalysts of various oxidative dehydrogenation reactions such as the formation of pyruvic acid from lactic acid [1–3], glyoxylic acid from glycolic acid [4] and glyoxal from ethylene glycol [5]. Further, compounds with open framework such as the olivine-type $LiFePO_4$ and the Nasicon-type $Li_3Fe_2(PO_4)_3$ have been proposed to be new candidates for the next generation of rechargeable lithium ion batteries because they are naturally abundant and offer benefits in terms of environmental benignity, cycling stability and high temperature capability [6–8].

In terms of basic research, these materials are featured by their high stability owing to the strong P–O covalency which stabilizes the anti-bonding Fe^{3+}/Fe^{2+} state through the Fe–O–P inductive effect. In the resulting structures, iron can adopt various coordination polyhedra (octahedron, trigonal bipyramid, tetrahedron, squared pyramid. . .) which often display with the phosphate groups variable connecting fashions giving rise to versatile frameworks which are considered as among the most perplexing ones in the mineral kingdom [9].

Our interest in these materials concerns the preparation compounds and the study of their structural and physical properties. As a part of this activity, we recently described the synthesis and characterization of some new alkali iron phosphates belonging to the A_2O–F_2O_3–P_2O_5 systems [10–13]. As an extension of the earlier work, we report here on the synthesis and characterization, by X-ray diffraction Mössbauer spectroscopy and magnetic susceptibility of a new iron phosphate of composition $Rb_9Fe_7(PO_4)_{10}$. Its main structural feature deals with the presence of Fe_2O_{10} units of corner-sharing FeO_6 and FeO_5 polyhedra.

2. Experimental

2.1. Synthesis

The $Rb_9Fe_7(PO_4)_{10}$ compound, examined in this work, was synthesized as single crystals in a flux of rubidium dimolybdate $Rb_2Mo_2O_7$. A starting mixture of 2.916 g (1.26×10^{-2} mol) of Rb_2CO_3, 7.141 g (1.71×10^{-2} mol) of $Fe(NO_3)_3{\cdot}9H_2O$, 3.334 g (2.5×10^{-2} mol) of $(NH_4)_2HPO_4$ and 0.363 g (0.25×10^{-2} mol) of MoO_3 was firstly dissolved in aqueous nitric acid and the resulting solution was evaporated to dryness by heating in air for 24 h at 353 K. The obtained dry residue was homogenized by grinding in an agate mortar, transferred into a platinum crucible and then heated in stages to 473, 673 and 873 K for 24 h at each stage. This process was followed by further grinding, melting for 1 h at 1173 K and cooling at a rate of $10^\circ\ h^{-1}$ to 673 K, then at a rate of $50^\circ\ h^{-1}$ to room temperature. Light pink and irregularly shaped crystals of $Rb_9Fe_7(PO_4)_{10}$ were obtained by washing the whole product with hot water to remove the flux.

2.2. Structural determination

The crystal structure of the $Rb_9Fe_7(PO_4)_{10}$ compound was determined from single X-ray data. A suitable crystal of dimensions 0.04 mn × 0.06 mm × 0.4 mm was selected for indexing and intensity data collection at room temperature on an

* Corresponding author. Tel.: +216 73500279.
E-mail address: mourad_hidouri@yahoo.fr (M. Hidouri).

0925-8388/$ – see front matter © 2010 Elsevier B.V. All rights reserved.
doi:10.1016/j.jallcom.2010.07.089

Table 1
Crystallographic data for $Rb_9Fe_7(PO_4)_{10}$.

Crystal data	
Chemical formula	$Rb_9Fe_7(PO_4)_{10}$
Formula weight ($g\,mol^{-1}$)	2109.9
Cell setting	Monoclinic
Space group	$P2_1/a$
a(Å)	9.886(4)
b(Å)	16.493(2)
c(Å)	13.437(2)
β(°)	110.49(3)
V(Å^3)	2052.3(9)
Z	2
ρ_{cal}($g\,cm^{-3}$)	3.41
Data collection	
Diffractometer	CAD4
λ (Å)	MoKα/0.71073
Absorption correction	Analytical
$T_{min/max}$	0.08/0.45
μ (mm^{-1})	13.52
Scan mode	$\omega/2\theta$
Scan speed	Variable
θ_{max}(°)	29.9
Standard reflections	Two measured every 2 h (no decay)
Unique reflections/R_{int}	5935/0.0001
Observed reflections	3674
Criterion for observed reflections	[Fo > 4σ(Fo)]
Indices	$-13 \le h \le 2$, $0 \le k \le 23$, $0 \le l \le 18$
F(0 0 0)	1970.0
Refinement	
Intensity correction	Lorentz-polarization
Resolution method	Direct method
Final R indices	$R_1 = 0.0508$; $wR_2 = 0.100$
Goodness-of-fit	$S = 1.047$ [Fo > 4σ(Fo)]
Number of parameters	303
Extinction coefficient	0.0013(2)
$(\Delta\rho)_{max,\,min}$/e Å^{-3}	1.64; −1.15
W	$W = 1/[\sigma^2(Fo^2) + (0.037P)^2]$ $P = [\max(Fo^2,0) + 2Fc^2]/3$

Enraf–Nonius CAD4 diffractometer using graphite monochromated MoKα radiation (λ = 0.7107 Å). Crystallographic data and experimental conditions for the structural refinement are compiled in Table 1. The unit cell parameters and the orientation matrix were determined by a least squares fit of 25 peak maxima in the range $8.86° \le \theta \le 12.63°$. The intensities of 5935 unique reflections were measured using the ω-2θ scan mode up to $2\theta_{max} = 60°$. Among them, 3674 were considered as observed according to the statistic criterion [$F_o^2 > 4\sigma(F_o^2)$]. No significant fluctuation was observed during the data collection, according to two standard reflections measured every 2 h. The intensities were corrected for Lorentz and polarization effects and analytical absorption correction was applied resulting in transmission factors in the range of 0.08–0.45. Based on statistical distribution and successful solution and refinement of the structure, the space group was determined to be $P2_1/a$. Direct methods [14] were used to locate the Rb and Fe atoms. Subsequently, the other atoms were progressively located from Fourier difference maps [15] after refinement of the known atomic positions. The occupancy factors of all the atoms were initially refined but the resultant values indicated full occupancies. None of the remaining peaks in the final difference Fourier synthesis could be refined as other atoms. The final cycle of refinement including anisotropic displacement parameters resulted in residuals of $R_1 = 0.051$, $wR_2 = 0.119$ and $S = 1.05$.

The atomic coordinates as well and complete structural data have been deposited with Fachiformationszentrum (FIZ) Karlsruhe, Informationsdienste ICSD, D-76344 Eggenstein–Leopoldshafen, Germany (e-mail: crystaldata@fiz-karlsruhe.de) under the CSD number 421907.

2.3. Characterization

The title compound was characterized by Differential thermal analysis (DTA), magnetic susceptibility and Mössbauer spectroscopy. DTA measurements were carried out under air atmosphere by heating up to 1273 K with a rate of 10 K mn^{-1}. Susceptibility measurements were preformed in the 2–300 K temperature range using a Quantum Design SQUID magnetometer at a constant applied magnetic field of 500 Oe. The sample was placed in a gelatin capsule fastened in a plastic straw for immersion in the SQUID system.

The ^{57}Fe Mössbauer measurements were performed with a constant acceleration HALDER–type spectrometer using a ^{57}Co source (Rh matrix) in transmission geometry. The spectra at 293 and 4.2 K were recorded using a variable temperature cryostat. The velocity was calibrated using pure iron metal as the standard material. The polycrystalline absorbers containing about 10 mg cm^{-2} of iron were used to avoid the experimental widening of the peaks.

3. Results and discussion

3.1. Description of the structure

The $Rb_9Fe_7(PO_4)_{10}$ structure closely resembles to that of the previously reported $Cs_{9-x}K_xFe_7(PO_4)_{10}$ phosphates [16]. Both have the same symmetry and very similar unit cell parameters. The projections of the title structure along the a and c axis (Fig. 1) show the open character of the $[Fe_7(PO_4)_{10}]_\infty$ framework forming intersecting tunnels, where the Rb^+ cations are located. This framework is built up from two distinct FeO_6 octahedra (Fe1 and Fe2), two distinct FeO_5 trigonal bipyramids (Fe3 and Fe4) and five distinct PO_4 tetrahedra. The $Fe1O_6$ and $Fe4O_5$ polyhedra are isolated while the $Fe2O_6$ and $Fe3O_5$ ones share one corner resulting in a Fe_2O_{10} unit. The connectivity of the Fe polyhedral units to the PO_4 tetrahedra is illustrated by Fig. 2. The $Fe1O_6$ octahedron shares its six corners with six different tetrahedra. The $Fe4O_5$ polyhedron is corner linked to three tetrahedra and edge-connected to one fourth tetrahedron. The Fe_2O_{10} unit is edge-shared with two tetrahedra and corner-connected with six tetrahedra, two of which are forming bridges between the Fe polyhedra forming the unit. The three-dimensional framework constructed in this way forms large intersecting tunnels that run along a and c. Within these tunnels the Rb^+ cation are totally occupying five distinct sites.

Table 2 gives main inter-atomic distances and angles in the structure. The octahedral environments of Fe1 and Fe2 are both distorted with that of Fe1 is more regular than that of Fe2. In fact, the Fe1–O distances ranging from 1.976(5) to 2.005(4) Å are significantly less dispersed than the Fe2–O ones scattering from 1.917(4) to 2.107(4) Å. The average distances ⟨Fe1–O⟩ = 1.995(5) Å and ⟨Fe2–O⟩ = 2.020(5) Å are close to 2.03 Å, calculated by Shannon for Fe^{3+} ions in octahedral oxygen environment [17]. The 5-fold coordination of the Fe3 and Fe4 atoms is not a common case in iron(III) phosphates. The Fe3 environment exhibits one extremely large Fe–O distance of 2.199(5) Å showing the geometry of the $Fe3O_5$ polyhedron to approximate a squared pyramid. Similar environment for five-coordinated Fe^{3+} ions has already been observed in $NaCaFe_3(PO_4)_4$ [18]. The $Fe4O_5$ polyhedron is less distorted than $Fe3O_5$ in view of the Fe4–O distances varying from 1.857(5) to 2.042(5) Å. The average distances within these two polyhedra ⟨Fe3–O⟩ = 1.964(5) Å and ⟨Fe4–O⟩ = 1.954(5) Å are in a good agreement with those 1.946 Å, 1.949 Å reported in $NaCaFe_3(PO_4)_4$. The PO_4 tetrahedra have P–O distances in the range of 1.484(5)–1.579(5) Å with an overall value of 1.540(5) Å, close to that 1.537 Å, typically observed in monophosphates [19]. The environments of the extra-framework rubidium cations were determined assuming a maximum Rb–O distance of 3.43 Å, according to Donnay and Allman [20]. These environments (Fig. 3) have coordination numbers varying from 7 to 9 with Rb–O distances scattering from 2.752(5) to 3.428(5) Å. Relatively high values of thermal displacements of these atoms indicate that these loosely bound ions perform thermally activated movements within the framework tunnels. Bond valence sum calculations performed by the Brown and Altermatt method [21] and given in Table 3 clearly indicate that all the cations are in good agreement with their formal oxidation states.

3.2. Thermal stability

Differential thermal analysis (DTA) data show that $Rb_9Fe_7(PO_4)_{10}$ is stable up to 1100 K and melts at 1140 K. Nevertheless, XRD patterns obtained at increasing temperatures

Table 2
Selected inter-atomic distances (Å) and angles (°) for $Rb_9Fe_7(PO_4)_{10}$.

$Fe(1)O_6$				$Fe2O_6$			
Fe1–O21 ×2	1.976(5)	O21–Fe1–O21	180.0(1)	Fe2–O52	1.917(5)	O52–Fe2–O53	97.0(2)
Fe1–O41 ×2	2.004(5)	O21–Fe1–O41	94.9(2)	Fe2–O53	1.933(5)	O52–Fe2–O31	87.8(2)
Fe1–O32 ×2	2.004(4)	O21–Fe1–O41	85.1(2)	Fe2–O31	1.969(4)	O53–Fe2–O31	102.7(2)
⟨Fe1–O⟩	1.995(5)	O21–Fe1–O41	85.1(2)	Fe2–O11	2.088(5)	O52–Fe2–O11	171.9(2)
B. V. S.	3.17	O21–Fe1–O41	94.9(2)	Fe2–O12	2.107(5)	O53–Fe2–O11	87.3(2)
		O41–Fe1–O41	180.0(1)	Fe2–O14	2.107(4)	O31–Fe2–O11	84.6(2)
		O21–Fe1–O32	89.5(2)	⟨Fe2–O⟩	2.020(5)	O52–Fe2–O12	90.3(2)
		O21–Fe1–O32	90.5(2)	B. V. S.	3.04	O53–Fe2–O12	162.6(2)
		O41–Fe1–O32	93.2(2)			O31–Fe2–O12	93.3(2)
		O41–Fe1–O32	86.7(2)			O11–Fe2–O12	87.6(2)
		O21–Fe1–O32	90.5(2)			O52–Fe2–O14	96.6(2)
		O21–Fe1–O32	89.5(1)			O53–Fe2–O14	93.7(2)
		O41–Fe1–O32	86.7(2)			O31–Fe2–O14	162.3(2)
		O41–Fe1–O32	93.5(2)			O11–Fe2–O14	89.9(2)
		O32–Fe1–O32	180.0(1)			O12–Fe2–O14	69.6(2)
$Fe(3)O_5$				$Fe(4)O_5$			
Fe3–O54	1.856(5)	O54–Fe3–O23	121.2(2)	Fe4–O24	1.857(5)	O24–Fe4–O33	111.1(2)
Fe3–O34	1.879(4)	O34–Fe3–O23	96.7(2)	Fe4–O33	1.909(5)	O24–Fe4–O42	102.8(2)
Fe3–O23	1.918(5)	O54–Fe3–O13	96.2(2)	Fe4–O42	1.935(4)	O33–Fe4–O42	95.4(2)
Fe3–O13	1.968(5)	O54–Fe3–O13	115.2(2)	Fe4–O43	2.030(4)	O24–Fe4–O43	102.1(2)
Fe3–O11	2.199(5)	O34–Fe3–O13	119.5(2)	Fe4–O44	2.041(5)	O33–Fe4–O43	87.3(2)
⟨Fe3–O⟩	1.964(5)	O23––Fe3–O13	97.6(2)	⟨Fe4–O⟩	1.954(5)	O42–Fe4–O43	152.0(2)
B. V. S.	3.01	O54–Fe3–O11	91.0(2)	B. V. S.	3.00	O24–Fe4–O44	110.4(2)
		O34–Fe3–O11	88.9(2)			O33–Fe4–O44	136.5(2)
		O23–Fe3–O11	166.7(2)			O42–Fe4–O44	87.6(2)
		O13–Fe3–O11	69.3(2)			O43–Fe4–O44	71.8(2)
$P(1)O_4$				$P(2)O_4$			
P1–O14	1.528(5)	O14–P1–O12	103.6(3)	P2–O22	1.486(5)	O22–P2–O21	112.4(3)
P1–O12	1.532(4)	O14–P1–O13	114.1(3)	P2–O21	1.523(5)	O22–P2–O23	111.7(3)
P1–O13	1.555(5)	O12–P1–O13	112.5(3)	P2–O23	1.562(5)	O21–P2–O23	107.4(3)
P1–O11	1.558(5)	O14–P1–O11	113.9(3)	P2–O24	1.579(5)	O22–P2–O24	112.3(3)
⟨P1–O⟩	1.543(5)	O12–P1–O11	113.6(3)	⟨P2–O⟩	1.542(5)	O21–P2–O24	109.2(3)
B. V. S.	4.90	O13–P1–O11	99.6(3)	B. V. S.	4.98	O23–P2–O24	103.4(3)
$P(3)O_4$				$P(4)O_4$			
P3–O32	1.521(5)	O32–P3–O31	110.7(3)	P4–O41	1.516(5)	O41–P4–O43	112.1(3)
P3–O31	1.523(5)	O32–P3–O33	111.9(3)	P4–O42	1.543(5)	O42–P4–O43	110.6(3)
P3–O33	1.537(5)	O31–P3–O33	107.7(3)	P4–O43	1.546(5)	O41–P4–O44	109.5(3)
P3–O34	1.549(5)	O32–P3–O34	106.3(3)	P4–O44	1.552(4)	O42–P4–O43	110.6(3)
⟨P3–O⟩	1.532(5)	O31–P3–O34	111.8(3)	⟨P4–O⟩	1.539(4)	O42–P4–O44	111.0(3)
B. V. S.	5.03	O33–P3–O34	108.5(3)	B. V. S.	4.94	O43–P4–O44	100.8(3)
$P(5)O_4$							
P5–O51	1.484(5)	O51–P5–O52	112.9(3)				
P5–O52	1.529(5)	O51–P5–O54	111.5(4)				
P5–O54	1.560(6)	O52–P5–O54	106.7(3)				
P5–O53	1.569(5)	O51–P5–O53	112.4(3)				
⟨P5–O⟩	1.536(5)	O52–P5–O53	105.0(3)				
B. V. S.	4.97	O54–P5–O53	108.0(3)				

Rb(1)		Rb(2)		Rb(3)	
Rb1–O22	2.752(5)	Rb2–O22	2.836(5)	Rb3–O52	3.030(5)
Rb1–O12	2.808(5)	Rb2–O51	2.870(5)	Rb3–O31	3.031(5)
Rb1–O51	2.811(5)	Rb2–O44	2.948(5)	Rb3–O53	3.036(5)
Rb1–O14	2.860(4)	Rb2–O14	3.026(5)	Rb3–O43	3.081(5)
Rb1–O32	3.030(5)	Rb2–O51	3.144(7)	Rb3–O23	3.129(5)
Rb1–O21	3.115(5)	Rb2–O53	3.241(5)	Rb3–O41	3.244(5)
Rb1–O44	3.151(5)	Rb2–O13	3.377(5)	Rb3–O21	3.299(5)
Rb1–O31	3.277(5)	Rb2–O42	3.490(5)	Rb3–O33	3.313(5)
Rb1–O11	3.428(5)				
B. V. S.	1.34	B. V. S.	0.94	B. V. S.	0.77
Rb(4)		Rb(5)			
Rb4–O22	2.868(5)	Rb5–O32	2.942(5)		
Rb4–O22	2.868(5)	Rb5–O43	3.008(5)		
Rb4–O13	3.111(5)	Rb5–O23	3.042(5)		
Rb4–O13	3.111(5)	Rb5–O24	3.046(5)		
Rb4–O12	3.144(5)	Rb5–O34	3.158(5)		
Rb4–O12	3.144(5)	Rb5–O41	3.160(5)		
Rb4–O54	3.425(6)	Rb5–O44	3.229(5)		
Rb4–O54	3.425(6)				
B. V. S.	0.85	B. V. S.	0.79		

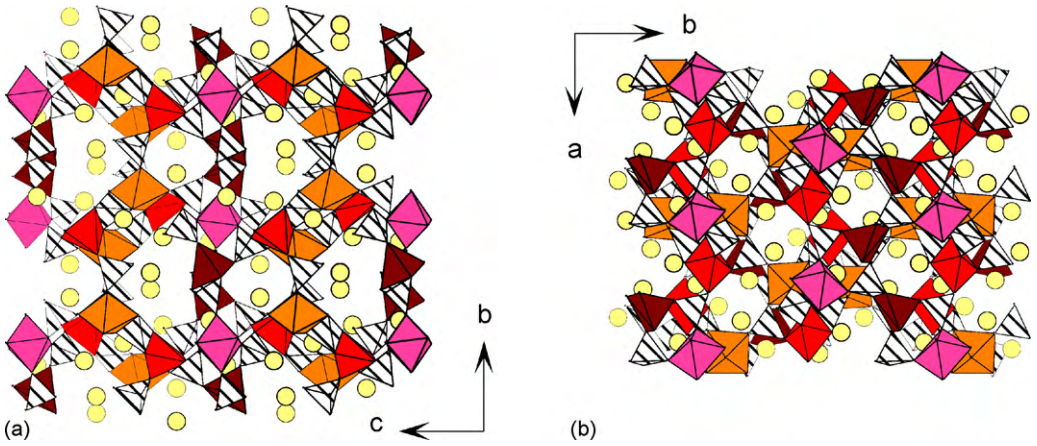

Fig. 1. Views of the structure along *a* (a) and *c* (b) showing the intersecting tunnels.

Table 3
Mössbauer spectrum for at 293 K.

Distribution	δ (mm/s)	Γ (mm/s)	Δ^a (mm/s)	% Experimental	% Theoretical	Coordination
DIS1	0.44	0.20	0.28	15	14.5	6
DIS2	0.41	0.20	0.33	25	28.5	6
DIS3	0.35	0.20	0.49	28	28.5	5
DIS4	0.36	0.20	0.46	32	28.5	5

[a] Δ (mm/s) is mean quadrupolar splitting.

only show similar diffraction peaks below 773 K. Above this temperature some changes at 823 K appear, probably related to a partial decomposition that was not detected by DTA. When the title phosphate was heated at 1073 K a brown product was obtained. A Rietveld analysis of its powder X-ray diagram show that it consists of two phases, a major phase identified as $Rb_9Fe_7(PO_4)_{10}$ and a minor phase which was not possible to identify it from the XRD pattern.

3.3. Magnetic susceptibility

The temperature dependencies of the molar magnetic susceptibility χ and its reciprocal χ^{-1} for $Rb_9Fe_7(PO_4)_{10}$ is illustrated by Fig. 4. These curves indicate a transition from paramagnetic to antiferromagnetic state at $T_N \approx 19$ K. Above T_N, the χ^{-1} plot is linear following the Curie–Weiss behavior. The derived Curie constant per iron atom $C = 4.48$ emu mol^{-1} K and effective paramagnetic moment $\mu = 5.99\,\mu_B$ are close to those $C = 4.37$ emu mol^{-1} K and $\mu = 5.92\,\mu_B$, expected for isolated Fe^{3+} (d^5) ions in high spin configuration. The Weiss temperature determined through a linear least squares extrapolation to zero has a negative value of $\theta_P = -64$ K, indicating that the exchange interactions which occur at low temperatures are of antiferromagnetic type.

3.4. Mössbauer spectroscopy

3.4.1. Room temperature study

The room temperature spectrum (Fig. 5) consists of a large dissymmetric signal which can be well described by the overlap of several doublets. From a first fit using Lorentzian profile lines, it was possible to distinguish two distinct symmetric doublets with isomer shifts and quadrupole splitting typical of Fe^{3+} ions in 6 and 5 coordination, respectively. However, a refinement using four distinct sites, in accordance with the crystallographic results was unsuccessful since it was not possible to distinguish between sites of identical coordination. In the other hand, an abnormal widening of the doublets was observed indicating the existence of a disorder around the iron sites. Tacking into account these results, a second fit was undertaken assuming four distributions assigned to the four crystallographic iron sites. The derived hyperfine parameters are given in Table 3. The isomer shifts for the DS1 and DS2 distributions ($\delta_1 = 0.44$ mm s^{-1}, $\delta_2 = 0.41$ mm s^{-1}) are typical of Fe^{3+} ions in distorted octahedral environments [22]. From a comparison of the

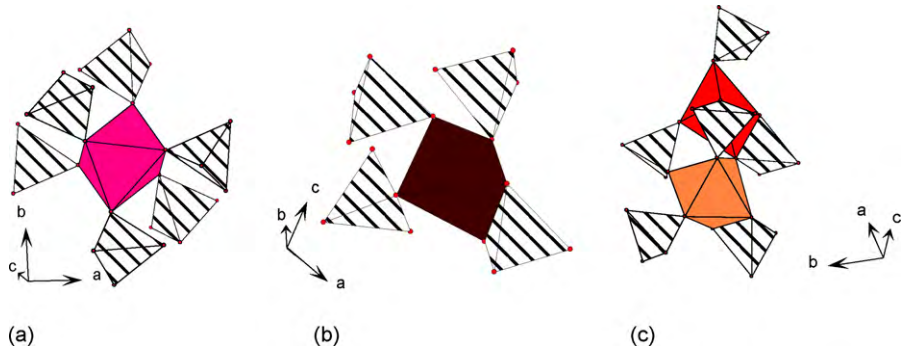

Fig. 2. The polyhedral environments of Fe1O6 (a), Fe4O5 (b) and Fe2O10 (c).

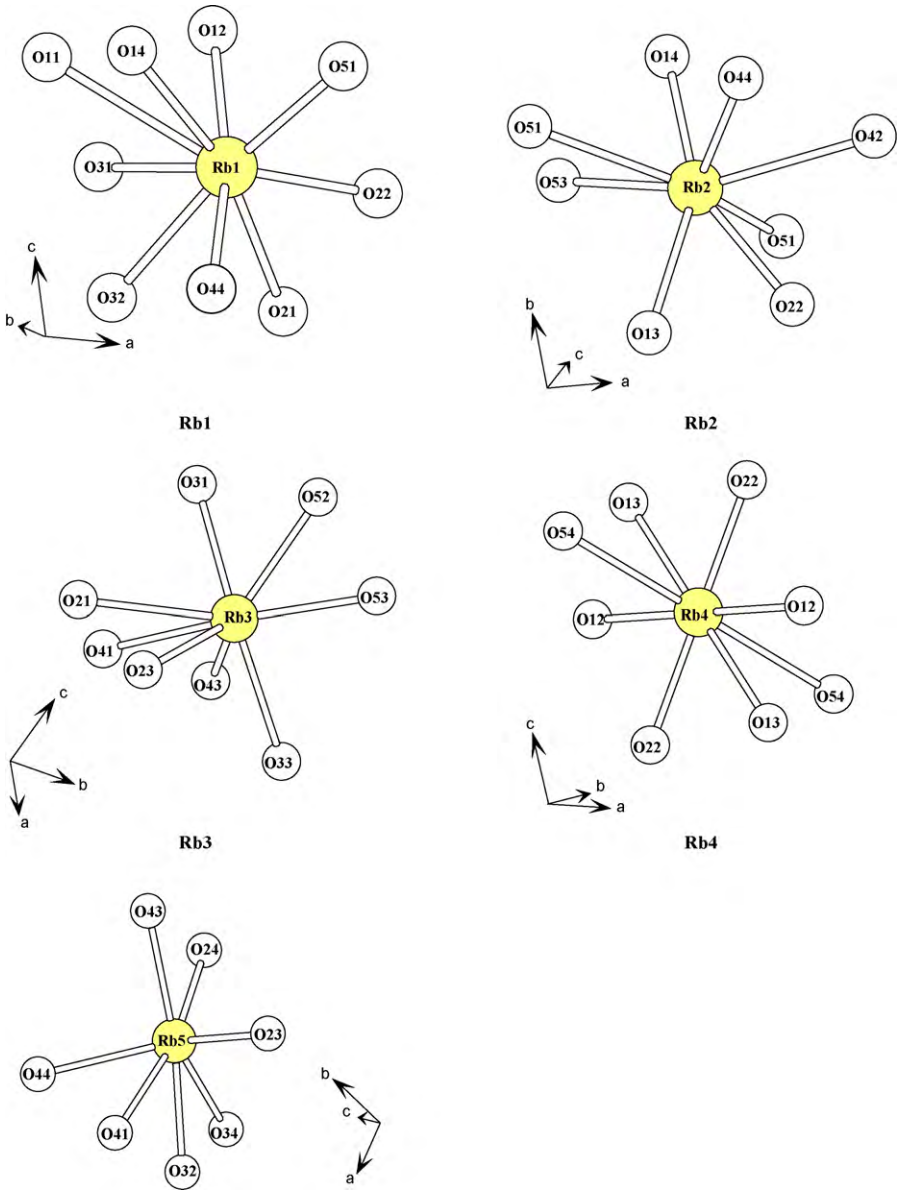

Fig. 3. The oxygen environments of the Rb^{+} cations.

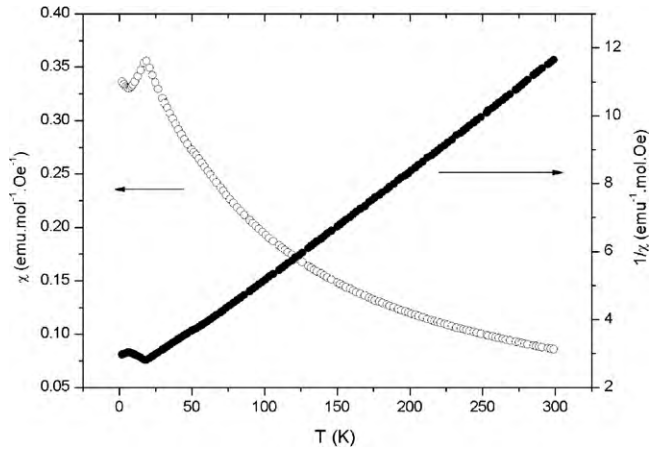

Fig. 4. Thermal variation of molar magnetic susceptibility and its inverse for Rb9Fe7(PO4)10.

relative populations, it was possible to attribute DS1 (15%) to the Fe1 site located at an inversion center and DS2 (25%) to the Fe2 site, occupying a general position. The quadrupolar splitting values show that DS1 ($\Delta_1 = 0.28\ \mathrm{mm\ s^{-1}}$) is slightly less distorted than DS2 ($\Delta_2 = 0.33\ \mathrm{mm\ s^{-1}}$). This result support that previously obtained by the crystallographic study which predicts a strong deformation

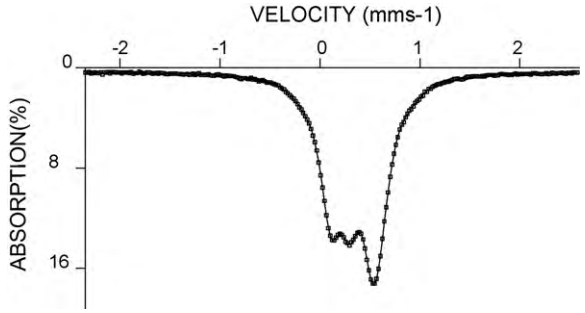

Fig. 5. The room temperature Mössbauer spectrum for Rb9Fe7(PO4)10.

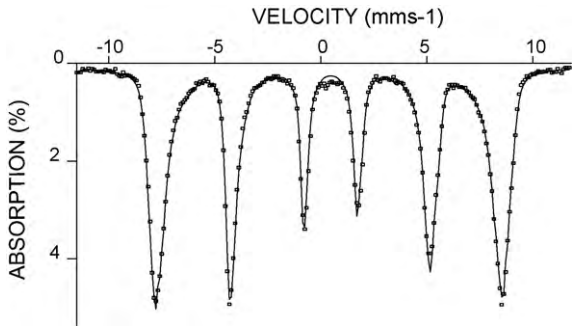

Fig. 6. The Mössbauer spectrum at 4.2 K.

Table 4
Mössbauer spectrum for for $Rb_9Fe_7(PO_4)_{10}$ at 4.2 K.

Distribution	δ (mm/s)	Γ (mm/s)	ε[a] (mm/s)	H[b] (T)	%	Coordination
DIS1	0.55	0.30	−0.08	51	42	6
DIS2	0.44	0.30	−0.02	49	58	5

[a] ε (mm/s) is electrical interaction parameter.
[b] H (T) is mean hyperfine field.

of the $Fe2O_6$ octahedron when compared to $Fe1O_6$. The DS3 and DS4 ($\delta_3 = 0.35\,mm\,s^{-1}$, $\delta_4 = 0.36\,mm\,s^{-1}$) are characteristic of ferric ions same ions in 5-fold coordination [22]. From a comparison of their qudrupolar splittings, one can assign DS3 ($\Delta_3 = 0.49\,mm\,s^{-1}$) to the highly distorted Fe3 site and DS4 ($\Delta_4 = 0.46\,mm\,s^{-1}$) to Fe4 of slightly less distortion.

3.4.2. Study at 4.2 K

The spectrum registered at 4.2 K (Fig. 6) consists of a sextet, characteristic of a magnetically ordered material. Due to the great widening of the doublets, the spectrum could be fitted assuming only two hyperfine field distributions. The derived hyperfine fields (Table 4) are rather similar (51 and 49 T), being typical of high spin Fe^{3+} ions near the saturation state. The isomer shifts 0.55 and 0.44 mm s^{-1} are slightly large with those obtained at room temperature and these differences [$\Delta(\delta) \approx 0.12\,mm\,s^{-1}$] can be attributed to thermal variation of the Doppler second order effect.

4. Conclusion

A new iron phosphate $Rb_9Fe_7(PO_4)_{10}$ has been isolated through a study of the Rb_2O–F_2O_3–P_2O_5 system and characterized by a combination of X-ray diffraction, magnetic susceptibility and Mössbauer spectroscopy. Its monoclinic structure consists of a complex three-dimensional network formed by isolated FeO_6 octahedra and FeO_5 bipyramids and Fe_2O_{10} units built up from a corner-sharing between one FeO_6 octahedron and one FeO_5 bipyramid. The connexion of these units via the phosphate tetrahedra generates a 3D open framework with crossing tunnels where the Rb^+ cations are located. This structural model was supported by a Mössbauer spectroscopy study undertaken at 293 and 4.2 K. The magnetic susceptibility indicated an antiferromagnetic transition at 19 K. The structural analogy of this compound with the $Cs_{9-x}K_xFe_7(PO_4)_{10}$ phosphates emphasizes the flexibility of the $[Fe_7(PO_4)_{10}]_\infty$ framework suggesting that it should be possible to prepare new isostructural phosphates including sodium or lithium.

Appendix A. Supplementary data

Supplementary data associated with this article can be found, in the online version, at doi:10.1016/j.jallcom.2010.07.089.

References

[1] M. Ai, K. Ohdan, Appl. Catal. A 150 (1997) 13.
[2] M. Ai, Appl. Catal. A 234 (2002) 235.
[3] M. Ai, Appl. Catal. A 232 (2002) 1.
[4] M. Ai, K. Ohdan, Stud. Surf. Sci. Catal. 110 (1997) 527.
[5] M. Ai, Catal. Today 52 (1999) 375.
[6] K.S. Nanjundaswamy, A.K. Padhi, J.B. Goodenough, S. Okada, H. Ohtsuka, H. Arai, J. Yamaki, Solid State Ionics 92 (1996) 1.
[7] A.K. Padhi, K.S. Nanjundaswamy, J.B. Goodenough, J. Electrochem. Soc. 144 (1997) 1188.
[8] C. Masquelier, A.K. Padhi, K.S. Nanjundaswamy, J.B. Goodenough, J. Solid State Chem. 135 (1998) 228.
[9] C. Gleitzer, Eur. J. Solid State Inorg. Chem. T 28 (1991) 77.
[10] B. Lajmi, M. Hidouri, M. Rzeigui, M. Ben Amara, Mater. Res. Bull. 37 (2002) 2407.
[11] B. Lajmi, Doctorat Thesis, Sciences University of Monastir, Tunisia (2004).
[12] B. Lajmi, M. Hidouri, M. Ben Amara, Acta Crystallogr. C58 (2002) i156.
[13] B. Lajmi, M. Hidouri, N. Gmati, A.B. Hammouda, A. Wattiaux, L. Fournés, J. Darriet, M. Ben Amara, Mater. Chem. Phys. 113 (2009) 372.
[14] A. Altomare, G. Cascarano, C. Giacovazzo et, A. Guagliardi, J. Appl. Crystallogr. 26 (1993) 343.
[15] G.M. Sheldrick, SHELXL97, A Program for the Solution of the Crystal Structures, University of Göttingen, Göttingen, Germany, 1997.
[16] G. Becht, S.-J. Hwu, Chem. Mater. 18 (2006) 4221.
[17] R.D. Shannon, Acta Crystallogr. A32 (1976) 751.
[18] M. Hidouri, B. Lajmi, A. Wattiaux, L. Fournes, J. Darriet, M.B. Amara, J. Alloys Compd. 358 (2003) 36.
[19] W.H. Bauer, Acta Crystallogr. B30 (1974) 1195.
[20] G. Donnay, R. Allman, Am. Miner. 55 (1970) 1003.
[21] I.D. Brown, D. Altermatt, Acta Crystallogr. B41 (1985) 244.
[22] F. Menil, J. Phys. Chem. Solids 46 (1985) 763.